Tribology International 210 (2025) 110798

Contents lists available at ScienceDirect

Tribology International

journal homepage: www.elsevier.com/locate/triboint

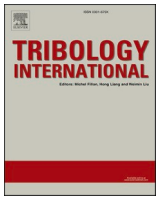

Elastohydrodynamic lubrication in rotational atherectomy: Fluid film thickness characteristics and reduction of vascular damage risk

Yuwen Liang, Urara Satake *, Toshiyuki Enomoto

Division of Mechanical Engineering, Graduate School of Engineering, Osaka University, 2-1, Yamada-oka, Suita, Osaka 565-0871, Japan

ARTICLE INFO

Keywords:
Elastohydrodynamic lubrication
Film thickness
Surgical device
Geometry improvement

ABSTRACT

In rotational atherectomy, a fluid film separates rotating burr and blood vessel, preventing vascular damage and involving elastohydrodynamic lubrication (EHL). Investigating fluid film thickness is necessary, as insufficient thickness increases vascular damage risk. This study examined damage depth on vascular phantom, revealing fluid film thickness characteristics and trends are similar to classical point contact EHL. The influence of burr and vascular phantom geometry was discussed with classical point contact EHL analysis, leading to a strategy: increasing burr's radius on tangential direction that can reduce damage risk by thickening fluid film. The findings demonstrate that classical point contact EHL provides valuable insights into this fluid film and can guide strategies for reducing vascular damage risk by improving fluid film thickness.

1. Introduction

Elastohydrodynamic lubrication (EHL) usually occurs under non-conformal contact conditions, where elastic deformation of the contact surfaces affects the lubrication process. EHL widely exists in mechanical components, such as roller bearings and gears, and plays a critical role in assessing mechanical damages. In recent decades, EHL analysis has been extended to biomedical field, providing valuable insights into biomedical lubrication processes and phenomena, and helping improve biomedical applications.

Cardiovascular diseases are among the leading causes of death worldwide. Atherosclerosis in coronary arteries often results in arterial stenosis, which restricts myocardial blood flow and contributes to severe cardiovascular diseases. Rotational atherectomy (RA) is a surgical procedure to prepare calcified plaque for restoring blood flow by using a high-speed rotating burr with a flexible shaft to ablate the calcified plaque [1]. While the burr primarily targets ablating calcified plaque, it may also come into contact with the blood vessel. In principle, the burr does not ablate blood vessel and cause mechanical damage [2], which is thought to be associated with elastohydrodynamic lubrication (EHL), the rotating burr drives the surrounding fluid to flow into the contact area between the burr and blood vessel, generating hydrodynamic pressure that can separate them. A sufficiently thick fluid film can effectively separate the rotating burr and blood vessel, preventing the grain on the burr contact with the vessel wall, as shown in Fig. 1.

Several studies have investigated the phenomenon by which the blood vessel avoids mechanical damage during RA. Nakao et al. [3] conducted experiments using boiled egg whites with various tools and assessed the compliance of the tools with the requirement of preventing vascular mechanical damage by observing egg whites remained intact, and concluded that the burr used in the surgery satisfies with the requirement; Kim et al. [4] validated that their designed tool does not mechanically damage the blood vessel by testing it on a silicone rubber block. They explained their results based on the relationship between the minimum film thickness that was calculated by empirical models in classical EHL and burr's grain protrusion. Additionally, Zheng et al. [5] thought their vascular phantom was not damaged by the surgical burr since the minimum film thickness, which was calculated by Hamrock and Dawson's empirical model of point contact EHL, exceeded the height of the burr's abrasive grain's protrusion.

However, surgical conditions can be complex, and mechanical damage may occur if the fluid film is too thin, allowing the burr's grains to contact and ablate the blood vessel. Researchers have cautioned that the burr can cause mechanical damage, which is a significant mechanism to cause vascular perforation, the most severe complication in RA [6,7]. To reduce this risk, contact between burr's grains and the blood vessel should be avoided. Theoretically, this can be realized by either increasing the fluid film thickness or reducing the grain protrusion. However, using burrs with small grain protrusion increases the risk of clogging when cutting hard calcified plaques, which are mainly contain

* Corresponding author.
E-mail address: satake@mech.eng.osaka-u.ac.jp (U. Satake).

https://doi.org/10.1016/j.triboint.2025.110798
Received 5 March 2025; Received in revised form 30 April 2025; Accepted 10 May 2025
Available online 13 May 2025

hydroxyapatite, severe clogging can occur under saline supplement [8]. Clogging potentially leads to serious complications such as platelet activation due to excessive heat and burr entrapment. As a result, increasing the film thickness is generally preferred over merely reducing the grain protrusion, but related studies remain scarce yet.

In EHL, the fluid film thickness is usually uneven and influenced by the motion and geometry of the contact solids, with thinner areas causing a higher risk of mechanical damage, even causing more severe mechanical damage. Therefore, understanding the characteristics and trends of film thickness between the burr and blood vessel under varying conditions is crucial for increasing the fluid film thickness and reducing mechanical damage risk. However, current studies mainly focus on the presence or absence of mechanical damage on vascular phantom in their experiments, explaining their results using the relationship between minimum film thickness calculated from empirical models and grain protrusion. This approach offers limited insights.

This study evaluated the vascular damage depth characteristics through phantom experiments to investigate the thickness characteristics of fluid film between the rotating burr and the blood vessel, as well as the influence of factors such as load force and burr's rotation speed on its trends. Results showed similarities with classical point contact EHL in both film thickness characteristics and trends. Therefore, it was thought that classical point contact EHL analysis can provide valuable insights into increasing film thickness between the burr and blood vessel to reduce vascular damage risk. Based on the analysis in point contact EHL, a strategy for thickening fluid film by improving contact geometry was proposed for reducing the vascular damage risk in RA surgery. Specifically, using a burr with a large radius of curvature in tangential direction was found to effectively increase the film thickness, even under unfavorable conditions, such as large loads or low rotation speeds.

2. Material and methods

2.1. Materials

Fig. 2(a) illustrates the overall setup, a spherical burr (D-60CB, Yanase Inc.) was used as the reference tool and an oval burr (D-60QB, Yanase Inc.) was used to test the proposed strategy for reducing vascular damage risk. Both burrs have 6 mm diameter and #140 abrasive grain size, whereas the oval burr is 10 mm in length. Scanning electron microscope (SEM) images (TM3000, Hitachi Inc.) in Fig. 2(b) show that both burrs have typical grain geometry of industrial burrs, bulk-shaped polyhedral grains with no specific orientation or preferred arrangement. No noticeable difference in grain geometry was observed between the spherical and oval burrs. The burr's size and grain size are larger than actual surgical burrs for facilitating causing damage on the vascular phantom in experiments. The shaft of burrs was stiff instead of flexible for better control. A high-speed spindle (HES810, Nakanishi Inc.) that provided burr's rotation was mounted on a machining center (AVJ-18, Yamazaki Mazak Corp.) that controlled feeding.

The tissue phantom inside the container comprised a vascular phantom, muscle phantom, mimic plaque, and water inside vascular phantom, as shown in Fig. 2(a). The silicone-made vascular phantom (Ecoflex 00–10, Smooth-On Inc.) had an elastic modulus of roughly 50 kPa, similar to the actual blood vessel; the muscle phantom was made of gelatin (Gelatin 21, Nitta Gelatin Inc.) that had a modulus around 2 kPa, approaches to muscle [9–11]. The vascular phantom was prepared as follows. Part A and part B of Ecoflex 00–10 were mixed in a 1:1 wt ratio, and the white pigment (Posilicone Inc.) with 4 % of the silicone mixture in weight was added for better observation. The mixture was then defoamed and poured into a cylindrical mold for making vascular phantom sized 55 mm in length and 4 mm in wall thickness. After curing at 60 °C for 2 hours, the vascular phantom was demolded and adhered to a PLA mimic plaque that was placed inside the container. The inside space of the container for containing the tissue phantom was 50 mm long in the X and Y directions and 60 mm high in the Z direction, as shown in Fig. 2(a). For the muscle phantom, gelatin powder was dissolved in 50°C water at a 1:9 wt ratio. After thorough mixing, the gelatin was poured into the container and cooled at 20°C for 6 hours. The thin fluid film (< 100 μm) between high-speed rotating burr and static vascular phantom results in a characteristic shear rate on the order of 10, 000 s^{-1} or higher. At such a high shear rate, blood shows Newtonian behavior and has a viscosity of around 1–1.5 mPa·s [12], which is close to water. Therefore, water (20 °C) was chosen to provide fluid environment. The entire setup was connected to a force sensor (9327 C, Kistler Inc.) and mounted on the machining center via jigs.

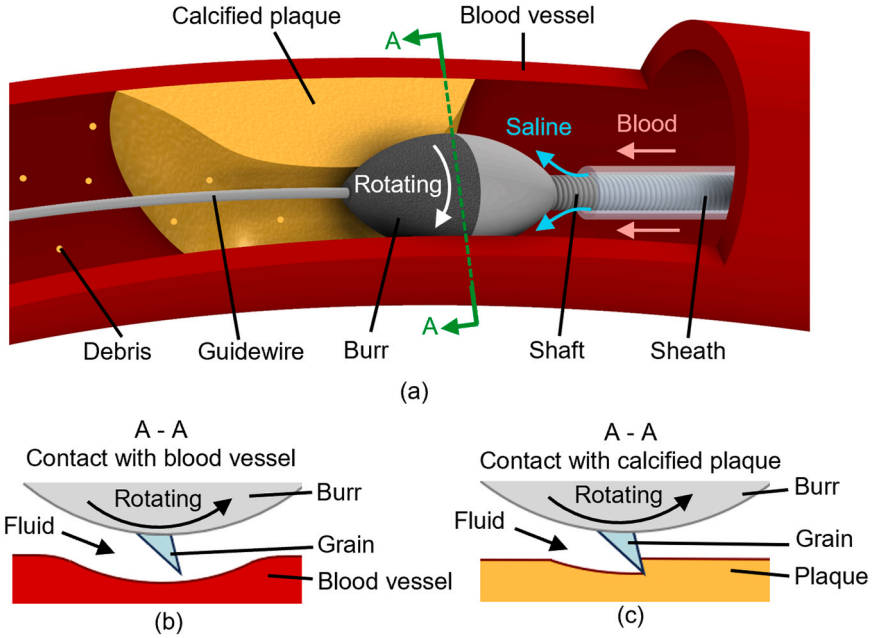

Fig. 1. (a) Schematic of ablating calcified plaque in the blood vessel by RA, (b) schematic of burr avoids ablating blood vessel, (c) schematic of the burr ablates calcified plaque.

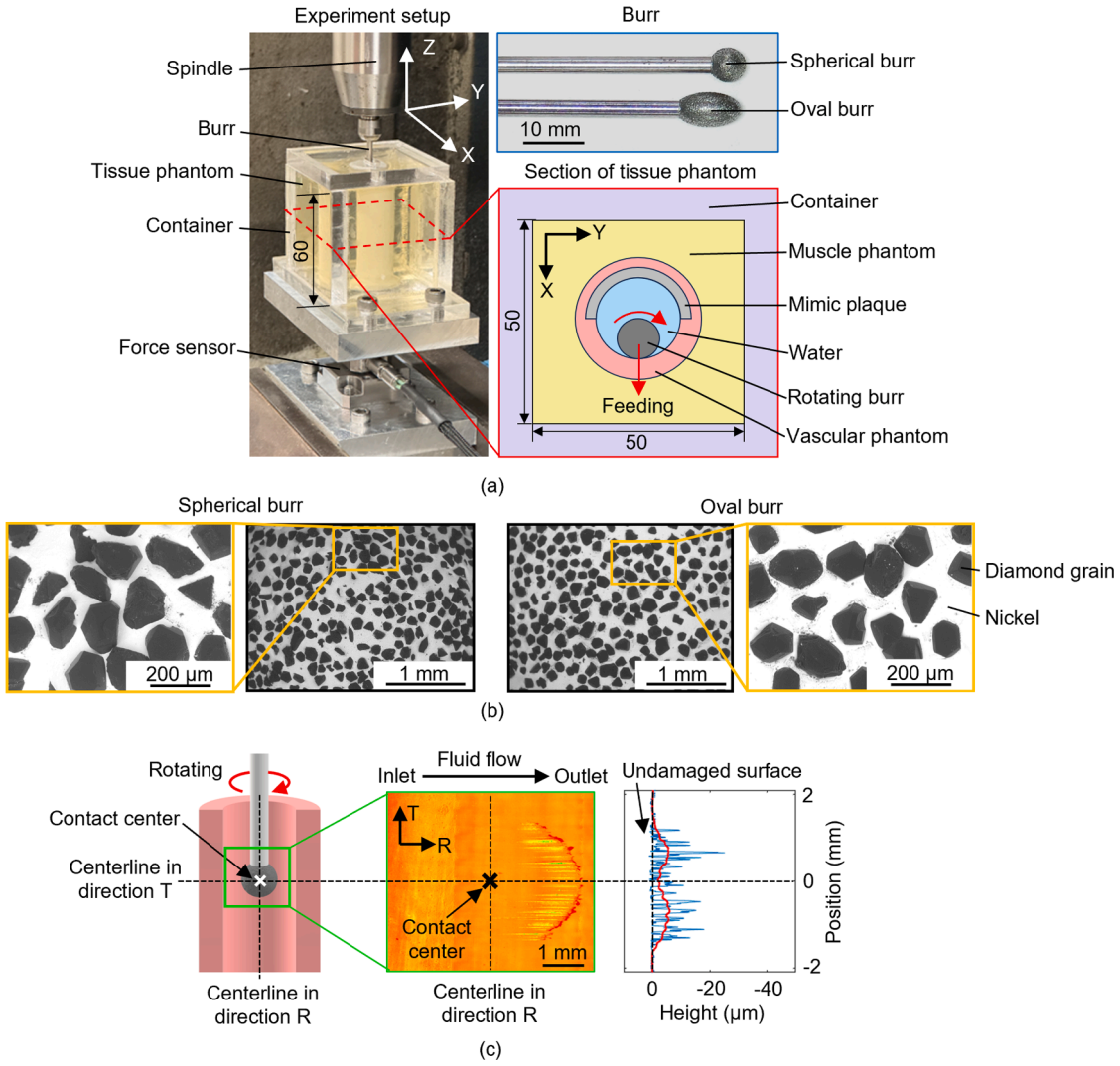

Fig. 2. (a) Experiment setup, (b) SEM images of spherical burr and oval burr, (c) experiment results, the damaged area on vascular phantom was processed to contour plot (middle) and projection profile (right).

2.2. Experiment procedure

In each experiment, the burr contacted the vascular phantom at least 18 mm below the phantom's top surface to avoid influence from the top surface. As shown in Fig. 2(a), the rotating burr was fed at 3 mm/min until a predetermined position was reached that can realize target force. For ensuring accurate control, the position was determined under non-rotating conditions. Immediately upon reaching the predetermined position that realized target load force, the burr was retracted. The reference load force was 0.10 N that possibly happen in surgeries [13], and additional forces of 0.02 N, 0.05 N, and 0.15 N were tested. The reference rotating speed was set to 35,000 rpm (line speed: 11.00 m/s), corresponds to rotating speed of around 140,000 rpm for a 1.5 mm surgical burr. Speeds of 25,000 rpm, 30,000 rpm, and 40,000 rpm were also tested. The reference lumen diameter was 12 mm, satisfies the recommended diameter ratio of burr to lumen [14] and the common ratio of arterial thickness to lumen diameter [15], 8 mm, 10 mm, and 15 mm lumen diameters were also tested. The oval burr was evaluated at the reference condition, as well as under large load force (0.15 N) and low rotating speed (25,000 rpm) conditions. To avoid occasional errors, experiments under each condition were performed three times.

2.3. Data analysis

After each test, two orthogonal centerlines were marked, one in the burr's rotating direction (direction R) and the other tangential to it (direction T), with the intersection serving as the contact center, as shown in Fig. 2(c). The vascular phantom was cut and observed under a laser microscope (VK-X200, Keyence Inc.). The cylindrical surface of the phantom was first numerically flattened in MultiFile Analyzer software (Keyence Inc.) for better visualization of the damage depth and then converted to a height matrix in MATLAB R2024b (MathWorks Inc.) for further processing. To quantify the damage depth, the damage depth was projected along direction R, i.e., the minimum height (maximum damage depth) along direction R, and then was corrected to flat the undamaged regions, shown as blue thin line in Fig. 2(c). This projection was then moving-averaged for highlighting depth characteristics in the direction T, shown as the red bold line in Fig. 2(c).

3. Results and discussion

3.1. Characteristics of fluid film thickness between burr and vessel wall

Under the reference condition, the representative damage result is shown in Fig. 3. In direction R, deep damage occurs near the outlet. In

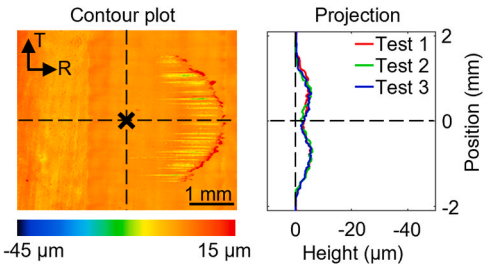

Fig. 3. Damage on the vascular phantom under reference condition.

direction T, deep damage occurs at two sides of the centerline. This pattern suggests that the fluid film is thinner near the outlet in direction R and at two sides of the centerline in direction T (corresponding to the two sides of burr's equator), which is similar to the film thickness distribution characteristics in classical point contact EHL [16].

Fluid film thickness characteristics in point contact EHL are analyzed along direction R and T separately, as shown in Fig. 4. In direction R, fluid is entrained into the contact area and experiences a significant pressure drop near the outlet [16], as shown in Fig. 4(b) and Fig. 4(c). This pressure drop causes a large pressure gradient that drives fluid flow in the same direction as burr's rotation, accelerating the fluid flow, as shown in Fig. 4(b). Regarding the fluid flow rate as constant by neglecting lateral flow in contact area, the film thickness decreases near the outlet. In the central contact area, the high pressure deforms the contact solids in a way that similar to dry contact, making the two deformed surfaces near parallel [17], as shown in Fig. 4(d). In direction T, side flow reduces the amount of fluid entering the contact area and thinning the fluid film at two sides of centerline [18], as shown in Fig. 4(e). Fluid loss can become severe near the ends of the contact area in direction T, where the fluid flows nearly tangentially to the boundary, as shown in Fig. 4(d), allowing fluid to easily bypass the contact area. Additionally, pressure is relatively low away from centerline in direction T. When the pressure is sufficiently small, the deformed solids no longer exhibit a deformation that makes the two surfaces near parallel, as in the central region. Instead, they separate more with increasing distance from the centerline, increasing fluid film thickness in outer areas in Fig. 4(e).

Experiments under different load forces and rotating speeds were conducted to better illustrate the similarities of thickness characteristics and trends of fluid film between the rotating burr and vascular phantom and those in classical point contact EHL. As shown in Fig. 5, heavier loads or lower rotating speeds result in deeper damage, with a more pronounced depth increase at the two sides compared to the centerline in direction T. For quantifying the damage depth, the largest depth, corresponding to the average depth of deepest damage at two sides of the centerline in direction T in the moving averaged projection, and the centerline depth, corresponding to the depth at the centerline in direction T of moving averaged projection, were evaluated. Table 1 and Table 2 show the quantified damage depth, which support the mentioned trends. The results indicate the fluid film thickness decreases under heavier loads or lower speeds, with a more pronounced pattern of thinner film at two sides of centerline in direction T, similar to classical point contact EHL [18].

In point contact EHL, as load force increases, pressure rises, which tends to squeeze fluid out of the contact area and resulting in a thinner fluid film. Higher pressure also enlarges the area where contact surfaces are near parallel that affected by side flow, causes this area to become closer to the contact boundary since pressure near the boundary also increases. Since fluid flows more tangentially to the contact boundary there, fluid loss becomes more severe and further thinning the fluid film. Conversely, increasing the burr's rotating speed enhances fluid entrainment, supporting a thicker fluid film and reducing the influence of fluid loss at the ends of contact area in direction T. This reduces the severity of thinning at two sides of the centerline and effectively increases fluid film thickness there.

3.2. *Strategy to reduce vascular damage by increasing fluid film thickness*

Experiments and analysis on load force and rotating speed demonstrate that reducing load force or increasing the burr's rotating speed can thicken fluid film and thereby reducing vascular damage risk, especially the thin film thickness at two sides of the centerline in direction T, where the risk of vascular damage is higher. However, large load forces may not be fully avoided in actual RA procedures, especially in curved blood vessel [13]. Additionally, excessively high rotating speeds can lead to cavitation or overheating, which increase the risk of complications such as non-reflow, coagulation, or myocardial infarction [19]. Therefore, additional strategies to increase film thickness are necessary.

Experimental results indicate that fluid film between the burr and blood vessel shows similar thickness characteristics and trends with

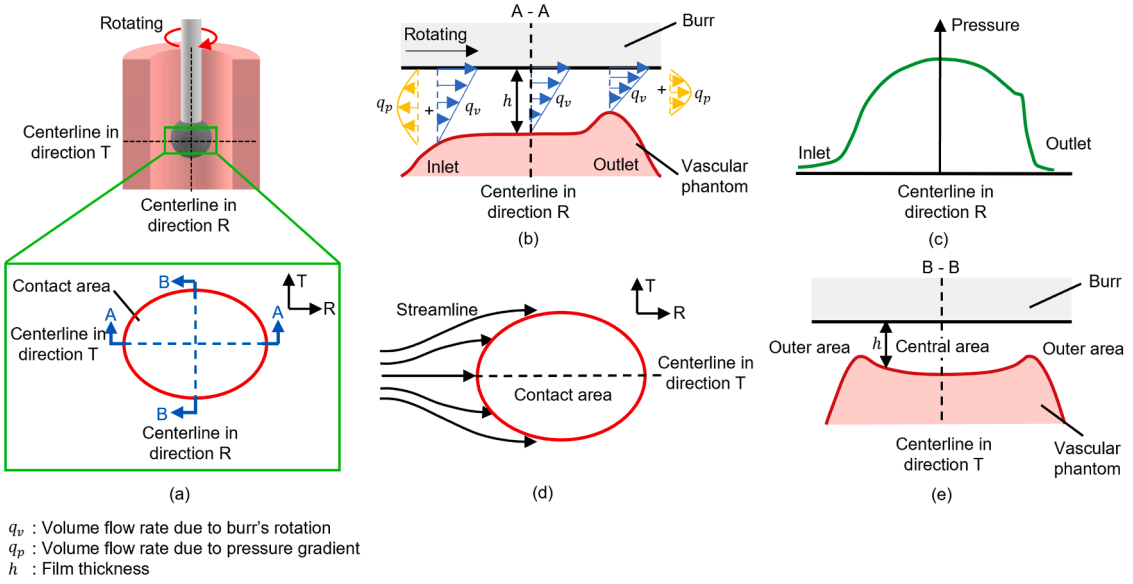

Fig. 4. Schematic of film thickness characteristics analysis in point contact EHL, (a) schematic of contact area and sections along centerlines in direction T and R, (b) film thickness distribution along direction R, (c) pressure distribution along direction R, (d) schematic of side flow, (e) film thickness distribution along direction T.

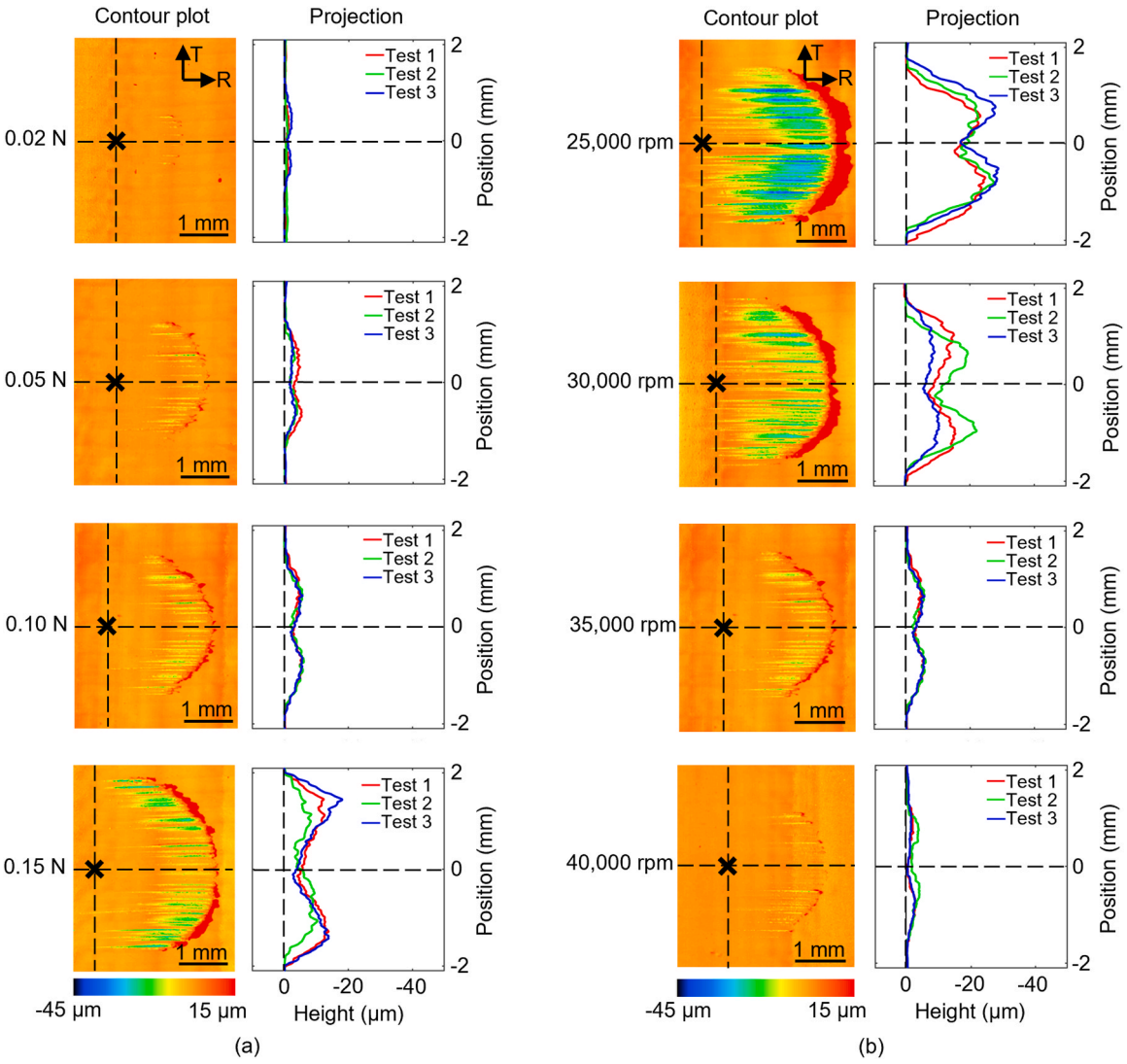

Fig. 5. (a) Experiment results under different load force, (b) experiment results under different rotating speed.

Table 1
Damage depth under different load force.

Load force (N)	Largest depth (μm)	Centerline depth (μm)
0.02	1.3	0.7
0.05	3.9	2.2
0.10	5.6	2.8
0.15	12.9	4.9

Table 2
Damage depth under different rotating speed.

Rotating speed (rpm)	Largest depth (μm)	Centerline depth (μm)
25,000	25.8	17.7
30,000	15.2	8.8
35,000	5.6	2.8
40,000	2.6	0.6

classical point contact EHL. Consequently, point contact EHL is thought to provide insights into understanding thickness characteristics and trends of fluid film between the burr and blood vessel, and can be applied for deriving the strategies to increase this fluid film thickness, especially the thin film thickness at the two sides of the centerline in direction T, to reduce the risk of vascular damage. In classical point contact EHL, apart from the side flow can reduce fluid entrainment into contact area at two sides of centerline in direction T, side flow can also reduce the overall fluid entrainment for forming the film, which does not facilitate forming a thick film [18]. Reducing side flow does not only reduce the thinning at two sides of centerline in direction T, but also increase the overall film thickness, thereby improving fluid film thickness and reducing vascular damage risk.

One way to reduce side flow is by adjusting the geometry of contact solids. The geometry of contact solids in point contact EHL can be described by equivalent radius in the direction T (R_t) and direction R (R_r), as shown in Fig. 6, Eqs. (1) and (2). In classical point contact EHL, a large radius ratio (R_t/R_r) tends to reduce the influence of side flow [18], thereby increasing fluid film thickness, including the thin film at two sides of the centerline. In Eqs. (1) and (2), R_{vr}, R_{br}, and R_{bt} are as defined in Fig. 6, while R_{vt} represents the radius of vascular phantom in direction T. In these experiments, its reciprocal is 0 since the vascular phantom has straight cylindrical lumen. The sign in Eq. (2) depends on blood vessel's curvature direction along direction T, "+" corresponds to a convex curve and "-" to a concave curve.

$$\frac{1}{R_r} = \frac{1}{R_{br}} - \frac{1}{R_{vr}} \tag{1}$$

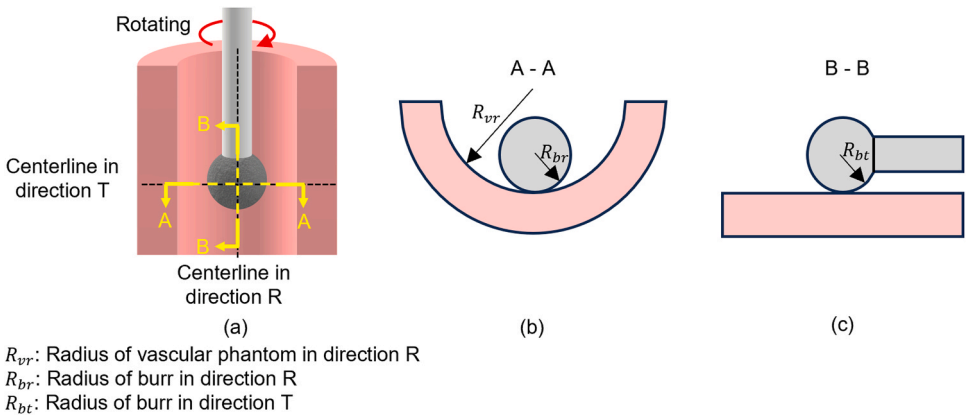

Fig. 6. Definition of the radius of burr and vascular phantom in direction T and R (a) schematic of the experiment, (b) section view on centerline in direction T, (c) section view on centerline in direction R.

$$\frac{1}{R_t} = \frac{1}{R_{bt}} \pm \frac{1}{R_{vt}} \tag{2}$$

To validate the effectiveness of increasing radius ratio, experiments were conducted using lumen diameters of 8 mm, 10 mm, 12 mm, and 15 mm, corresponding to radius ratios of 0.25, 0.4, 0.5, and 0.6 separately. As shown in Fig. 7 and Table 3, increasing the lumen diameter from 8 mm to 12 mm consistently reduces both the centerline depth and the largest depth, indicating the film thickness thickens at both the centerline and at two sides of centerline. However, at 15 mm, the largest depth increases while the centerline depth decreases compared to 12 mm, suggesting the fluid film thickness at centerline thickens while fluid film at two sides of the centerline becomes thinner.

Results can be explained from the combined effects of reduced side flow due to larger radius ratio and increased contact pressure due to smaller contact area at larger lumen diameters. Though larger lumen diameter leads to a larger radius ratio, it results in smaller contact area and larger contact pressure [20], which does not facilitate forming thick fluid film. When the lumen diameter increases from 8 mm to 12 mm, the increasing radius ratio provides a net benefit: both film thickness at the centerline or at the sides of centerline become thick despite the contact pressure increases, suggesting the effectiveness of increasing radius ratio. However, when lumen diameter increases to 15 mm, the high pressure may outweigh the advantage of reduced side flow at two sides by increasing radius ratio, making them more prone to thinning, even as the centerline film thickens, indicating the reduced side flow. Therefore, when designing strategies to increase film thickness between the burr and vascular phantom, the effects of contact area and contact pressure should also be considered.

3.3. Proposition of burr's shape design to reduce vascular damage

Reducing burr's radius in direction R is one way to achieve a larger radius ratio. However, simply reducing this radius may not always be feasible since it can reduce the contact area and increase contact pressure, which can potentially lead to a thinner fluid film that increases vascular damage risk. Additionally, surgical guidelines recommend a burr-to-lumen diameter ratio of 0.5–0.6 [14], meaning that a burr with a very small diameter may not effectively prepare calcified plaque. A more effective strategy is to increase the burr's radius of curvature in the direction T (R_{bt}). This approach not only reduces side flow loss by increasing radius ratio but also enlarges the contact area that reduces contact pressure. As analyzed, both factors contribute to forming a thicker fluid film, including the thin fluid film at the two sides of the centerline in the direction T.

This strategy was tested by using the 10 mm long oval burr that has a 9 mm radius of curvature in direction T, achieving a radius ratio of 1.5

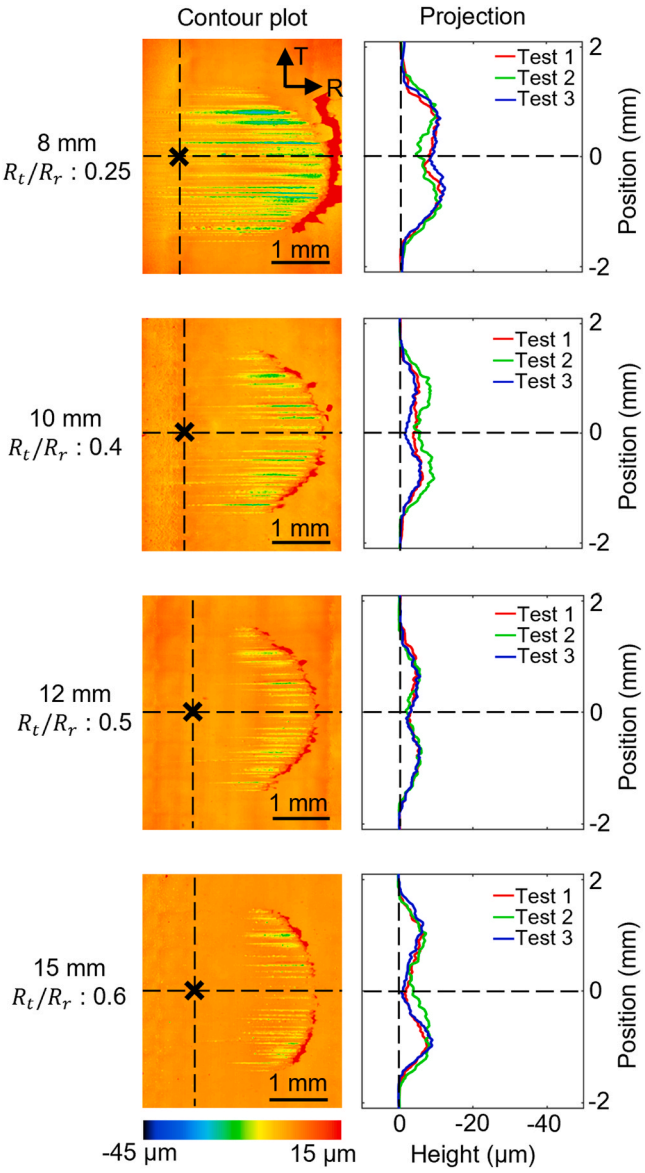

Fig. 7. Experiment results of different lumen diameters and radius ratios.

Table 3
Damage depth at different lumen diameter.

Lumen diameter (mm)	Radius ratio	Largest depth (μm)	Centerline depth (μm)
8	0.25	11.0	7.1
10	0.4	6.6	3.4
12	0.5	5.6	2.8
15	0.6	7.6	2.3

with a vascular phantom that has 12 mm lumen diameter. In addition to the reference condition, tests were conducted under large load force (0.15 N) and low rotating speed (25,000 rpm) conditions, which commonly increase vascular damage risk due to thin film thickness but can occur in RA, such as the accidental large load force or the use of low rotating speed to increase the lumen gain [21]. Fig. 8 and Table 4 show that, under all tested conditions, the oval burr reduced the centerline depth and largest depth compared to the spherical burr, confirming that increasing R_{bt} can effectively increase the fluid film thickness, especially at two sides of centerline, to reduce the vascular damage risk. Given its simplicity, such a design that proposed from point contact EHL analysis has a notable potential for easy adoption in actual surgeries, effectively reducing vascular damage risk in RA.

3.4. Limitations and future work

Water was used as fluid medium in this study. Although blood exhibits Newtonian behavior and its viscosity is close to water at a high shear rate, as mentioned in Section 2.1, blood may show different characteristics compared to water since real blood contains complex components, such as cells and plaque debris in RA surgery, which may cause the differences between the experimental results in this study and actual surgical conditions. Therefore, further investigation is necessary.

Though the influence of abrasive grain geometry was ignored in this study, as both spherical and oval burrs used in the experiments had the same grain size and showed no noticeable grain geometric differences, as described in Section 2.1, the geometry of abrasive grains may affect the performance of RA surgery. Future studies should investigate the influence of grain geometric characteristics such as shape, orientation, and arrangement.

Table 4
Damage depth of spherical burr and oval burr.

Condition	Burr's shape	Radius ratio	Largest depth (μm)	Centerline depth (μm)
Reference	Spherical	0.5	5.6	2.8
	Oval	1.5	1.1	0.1
Large load force	Spherical	0.5	12.9	4.9
	Oval	1.5	1.4	0.3
Low rotating speed	Spherical	0.5	25.8	17.7
	Oval	1.5	3.2	1.7

Furthermore, the present experimental study demonstrates that EHL analysis can offer valuable insights into RA surgery and surgical device improvement. In EHL, numerical simulations can provide localized information, in-depth and detailed analysis, that are difficult to obtain through experiments only. Therefore, incorporating EHL numerical simulations for RA surgery into future research is expected to enhance the understanding of RA process and contribute to surgical device development.

4. Conclusion

This study investigated characteristics and trends of fluid film thickness between the burr and blood vessel by investigating the damage depth on the vascular phantom in experiments simulating RA. The results suggest the film thickness between the rotating burr and vascular phantom show the similar characteristics and trends to classical point contact EHL. Specifically, the fluid film tends to be thinner near the outlet in the rotating direction and at two sides of centerline in direction T (corresponding to burr's equator). Additionally, fluid film thickness decreases with increasing load force or decreasing rotating speed. These findings indicate that point contact EHL provides valuable insights into characteristics and trends of fluid film thickness between the burr and blood vessel in rotational atherectomy.

Based on classical point contact EHL analysis, strategies to reduce vascular damage risk by increasing the fluid film thickness, particularly at two sides of centerline, were proposed by considering the radius ratio

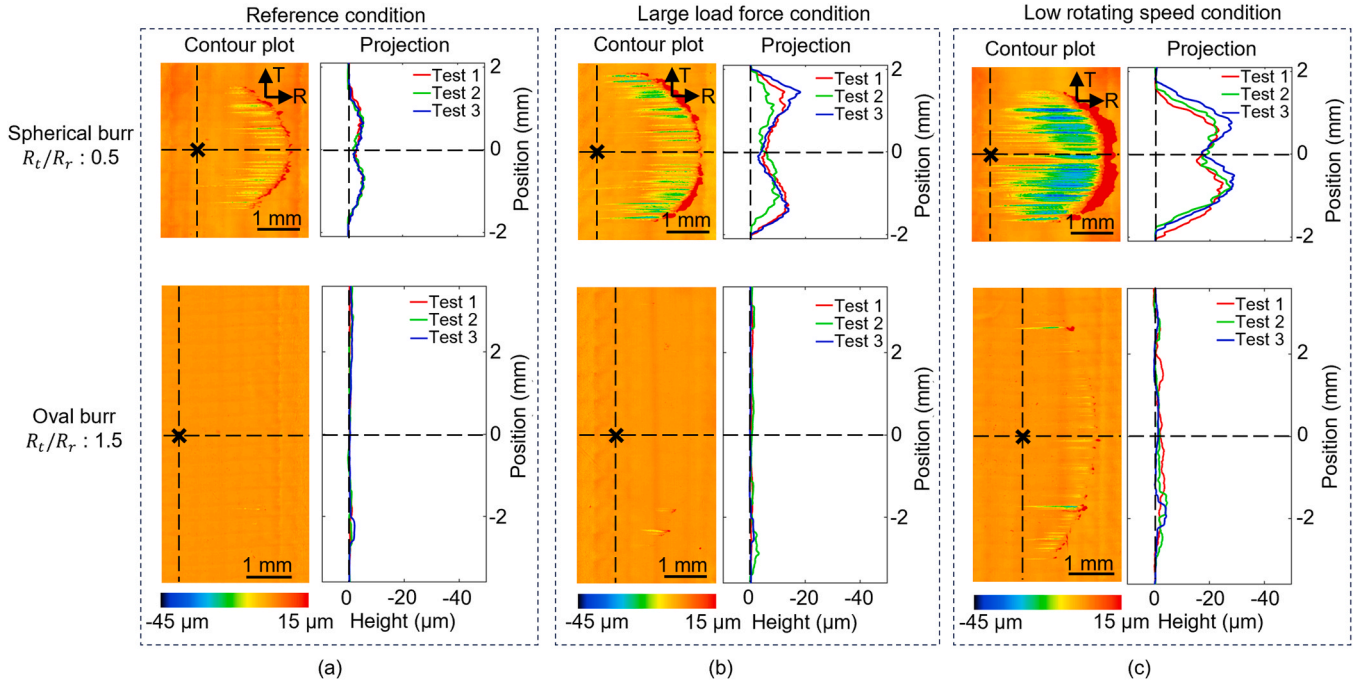

Fig. 8. Experiment results of spherical burr and oval burr under (a) reference condition, (b) large load force condition, and (c) low rotating speed condition.

of contacting burr and vascular phantom. Experimental results confirmed the effectiveness of this method and showed the need to consider the influence of contact area and pressure when improving contact geometry. Based on these findings, using a burr with a larger radius of curvature in the tangential direction emerged as a simple and practical solution. It takes advantage of both large radius ratio and low contact pressure in thickening fluid film and was experimentally verified to significantly increase fluid film thickness and reduce vascular damage risk.

Overall, this study demonstrates that point contact EHL provides valuable insights into characteristics and trends of film thickness between burr and blood vessel in RA and deriving effective strategies to reduce vascular damage risk.

CRediT authorship contribution statement

Enomoto Toshiyuki: Writing – review & editing, Investigation. **Satake Urara:** Writing – review & editing, Investigation, Funding acquisition. **Liang Yuwen:** Writing – original draft, Project administration, Methodology, Data curation, Conceptualization.

Declaration of Competing Interest

The authors declare that they have no known competing financial interests or personal relationships that could have appeared to influence the work reported in this paper.

Acknowledgement

This work was partially supported by Grant-in-Aid for Scientific Research (KAKENHI) from Japan Society for the Promotion of Science (JSPS), Proposal No. JP22K03843.

Data availability

Data will be made available on request.

References

[1] Rozenbaum Z, Takahashi T, Kobayashi Y, Bliagos D, Menegus M, Colombo A, et al. Contemporary technologies to modify calcified plaque in coronary artery disease. Prog Cardiovasc Dis 2021;69:18–26. https://doi.org/10.1016/j.pcad.2021.07.003.
[2] Dahdouh Z, Abdel-Massih T, Roule V, Sarkis A, Grollier G. Rotational atherectomy as endovascular haute couture: a road map of tools and techniques for the interventional management of burr entrapment. J Interv Cardiol 2013;26:586–95. https://doi.org/10.1111/joic.12075.
[3] Nakao M, Tsuchiya K, Maeda W, Iijima D. A rotating cutting tool to remove hard cemented deposits in heart blood vessels without damaging soft vessel walls. CIRP Ann 2005;54:37–40. https://doi.org/10.1016/S0007-8506(07)60044-4.
[4] Kim MH, Kim HJ, Kim NN, Yoon HS, Ahn SH. A rotational ablation tool for calcified atherosclerotic plaque removal. Biomed Micro 2011;13:963–71. https://doi.org/10.1007/s10544-011-9566-y.
[5] Zheng Y, Liu Y, Liu Y, Shih AJ. Experimental investigation of the grinding force in rotational atherectomy. Procedia Manuf 2016;5:838–48. https://doi.org/10.1016/j.promfg.2016.08.069.
[6] Taniguchi Y, Sakakura K, Jinnouchi H, Tsukui T, Fujita H. Rotational atherectomy to left circumflex ostial lesions: tips and tricks. Cardiovasc Inter Ther 2023;38:367–74. https://doi.org/10.1007/s12928-023-00941-y.
[7] Wang Y-H, Chen W-J, Chen Y-W, Lai C-H, Su C-S, Chang W-C, et al. Incidence and mechanisms of coronary perforations during rotational atherectomy in modern practice. J Interv Cardiol 2020;2020:1894389. https://doi.org/10.1155/2020/1894389.
[8] Mizutani T, Satake U, Enomoto T. Surgical diamond wheels for minimally invasive surgery in bone resection under small quantity of coolant supply. Precis Eng 2019;56:80–6. https://doi.org/10.1016/j.precisioneng.2018.09.015.
[9] Manish V, Arockiarajan A, Tamadapu G. Influence of water content on the mechanical behavior of gelatin based hydrogels: synthesis, characterization, and modeling. Int J Solids Struct 2021;233:111219. https://doi.org/10.1016/j.ijsolstr.2021.111219.
[10] McKee CT, Last JA, Russell P, Murphy CJ. Indentation versus tensile measurements of Young's modulus for soft biological tissues. Tissue Eng Part B Rev 2011;17:155–64. https://doi.org/10.1089/ten.teb.2010.0520.
[11] Vaicekauskaite J, Mazurek P, Vudayagiri S, Skov AL. Mapping the mechanical and electrical properties of commercial silicone elastomer formulations for stretchable transducers. J Mater Chem C 2020;8:1273–9. https://doi.org/10.1039/c9tc05072h.
[12] Munter WA, Stein PD. Newtonian behavior of blood at high rates of shear. Biorheology 1973;10:501–8. https://doi.org/10.3233/BIR-1973-10401.
[13] Zheng Y, Lyu J, Liu Y, Lo J, Susamaz A, Gurm HS, et al. Grinding wheel motion and force during plaque removal by rotational atherectomy in angulated coronary artery. Proc ASME 2018 13th Int Manuf Sci Eng Conf, Coll Station, Tex, Usa 2018. https://doi.org/10.1115/MSEC2018-6686.
[14] Tomey MI, Kini AS, Sharma SK. Current status of rotational atherectomy. JACC Cardiovasc Inter 2014;7:345–53. https://doi.org/10.1016/j.jcin.2013.12.196.
[15] Keegan J. Coronary artery wall imaging. J Magn Reson Imaging 2015;41:1190–202. https://doi.org/10.1002/jmri.24766.
[16] Spikes H. Basics of EHL for practical application. Lubr Sci 2015;27:45–67. https://doi.org/10.1002/ls.1271.
[17] Hooke CJ. Calculation of clearances in soft point contacts. J Tribol 1988;110:167–73. https://doi.org/10.1115/1.3261558.
[18] Venner CH, Lubrecht AA. Revisiting film thickness in slender elasto-hydrodynamically lubricated contacts. Proc Inst Mech Eng Part C J Mech Eng Sci 2010;224:2549–58. https://doi.org/10.1243/09544062JMES2316.
[19] Zotz RJ, Erbel R, Philipp A, Judt A, Wagner H, Lauterborn W, et al. High-speed rotational angioplasty-induced echo contrast in vivo and in vitro optical analysis. Cathet Cardiovasc Diagn 1992;26:98–109. https://doi.org/10.1002/ccd.1810260205.
[20] Hamrock BJ, Dowson D. Isothermal elastohydrodynamic lubrication of point contacts: part 1—theoretical formulation. J Lubr Technol 1976;98:223–8. https://doi.org/10.1115/1.3452801.
[21] Yamamoto T, Yada S, Matsuda Y, Otani H, Yoshikawa S, Sasaoka T, et al. A novel rotablator technique (low-speed following high-speed rotational atherectomy) can achieve larger lumen gain: evaluation using optimal frequency domain imaging. J Interv Cardiol 2019;2019:9282876. https://doi.org/10.1155/2019/9282876.